Overview of ATLAS forward proton detectors: status, performance, and new physics results

Savannah Clawson[a,*] **on behalf of the ATLAS collaboration**

[a]*Deutsches Elektronen-Synchrotron (DESY),*
Notkestr. 85, Hamburg, Germany

E-mail: savannah.clawson@desy.de

A key focus of the physics programme at the LHC is the study of head-on proton-proton collisions. However, an important class of physics can be studied for cases where the protons narrowly miss one another and remain intact. In such cases, the electromagnetic fields surrounding the protons can interact producing high-energy photon-photon collisions. Alternatively, interactions mediated by the strong force can also result in intact forward scattered protons, providing probes of quantum chromodynamics (QCD). In order to aid identification and provide unique information about these rare interactions, instrumentation to detect and measure protons scattered through very small angles is installed in the beam pipe far downstream of the interaction point. We describe the ATLAS Forward Proton (AFP) 'Roman Pot' detector, including its performance and status. The physics interest, as well as the newest results on photon-induced interactions, are also discussed.

The European Physical Society Conference on High Energy Physics (EPS-HEP2023)
21-25 August 2023
Hamburg, Germany

---

[*]Speaker

1. The ATLAS Forward Proton detector

The ATLAS Forward Proton (AFP) detector [1] is an extension of the ATLAS detector [2] at the Large Hadron Collider (LHC) [3] in the very forward region with the aim of measuring the energy loss and momentum of protons originating from diffractive and photon-induced processes at the ATLAS interaction point (IP1). Protons that have undergone scattering and remain intact, such that their energy E_{proton} is less than the nominal LHC beam energy E_{beam}, are sufficiently separated from the nominal beam orbit due to the LHC magnetic elements that they can be intercepted by so-called 'Roman Pot' (RP) systems inserted into the beam pipe aperture. The AFP detector consists of four separate RP stations, with two 'NEAR' stations located at $z = \pm205$ m and two 'FAR' stations located at $z = \pm217$ m from IP1, where the z-axis coincides with the beam axis. A schematic of the AFP stations, their location and the ATLAS coordinate system[1] are shown in Figure 1.
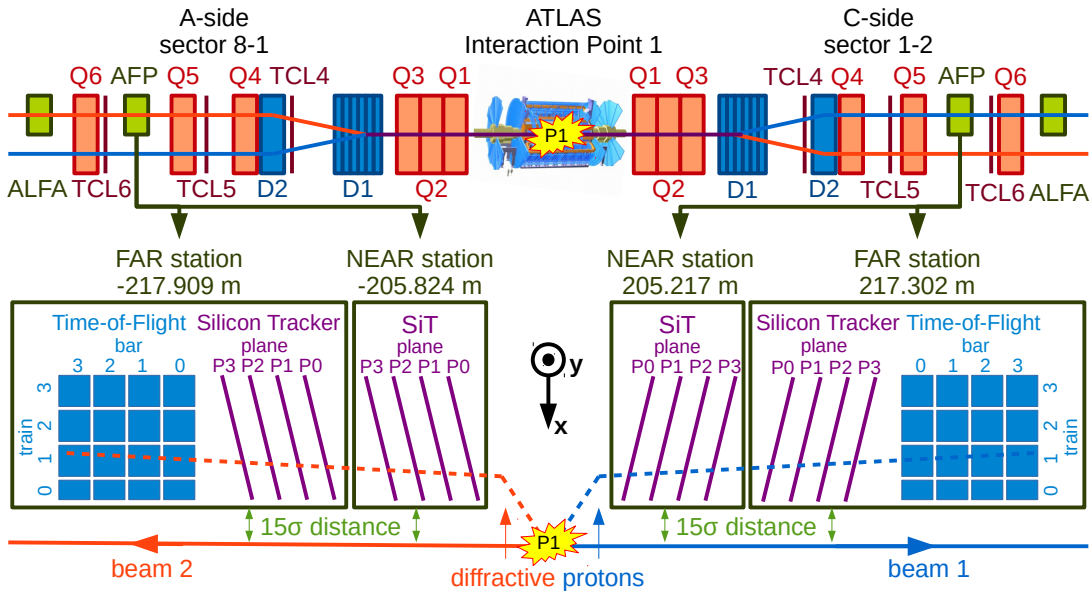

Figure 1: A schematic of the ATLAS Forward Proton (AFP) detector stations and their location relative to the ATLAS interaction point (IP1). The NEAR stations are located at roughly $z = \pm205$ m and the FAR stations roughly $z = \pm217$ m from IP1. All four stations have 4 planes of 3D silicon pixel trackers (SiT) while the outer stations have additional Cherenkov radiation time-of-flight (ToF) detectors. The aim of all stations is to measure intact protons that have undergone scattering at IP1. Figure taken from Ref. [4].

Each of the four stations houses four planes of edgeless silicon-tracking (SiT) sensors, consisting of 336×80 3D silicon pixels with an individual pixel area of $50 \times 250\,\mu m^2$. The planes have a depth of 230 μm in the beam direction and are separated by a distance of $\Delta z = 9$ mm. The short-pixel direction is set along the x-axis which is the predominant axis along which protons that have

---

[1]ATLAS uses a right-handed coordinate system with its origin at the nominal interaction point in the centre of the detector and the z-axis coinciding with the axis of the LHC beam pipe. The x-axis points from the interaction point to the centre of the LHC ring, and the y-axis points upward. The pseudorapidity is defined in terms of the polar angle θ as $\eta = -\ln\tan(\theta/2)$, and ϕ is the azimuthal angle around the beam pipe relative to the x-axis. The angular distance is defined as $\Delta R = \sqrt{(\Delta\eta)^2 + (\Delta\phi)^2}$.

undergone energy loss are deflected. Any divergence of protons along the long-pixel direction (y) is due to proton transverse momentum and non-zero crossing angle at IP1. The resolution in x is further improved by tilting the planes at a 14° angle about the y-axis so as to maximise charge sharing between pixels. This allows interpolation between two neighbouring pixels, improving the resolution to roughly $\sigma_x = 6\,\mu\text{m}$ [5].

The two FAR stations also house high-resolution timing detectors which aim to measure the proton time-of-flight (ToF) between IP1 and AFP. These detectors are designed to improve background suppression during high-luminosity data-taking and are located immediately behind the SiT planes on the outer side of the station. They consist of Cherenkov-scintillating L-shaped quartz bars (LQ-bars) [6], shown in Figure 2a. Four such LQ-bars are placed one after the other to form a 'train' parallel to the forward proton trajectory and each AFP-ToF detector has four trains, equaling sixteen bars in total which can be seen in Figure 2b. The transverse size of the LQ bars varies between 3–5 mm with increasing distance from the beam. The end of each light-guide arm is attached to a micro-channel plate multi-anode photo-multiplier (PMT) with 16 channels which converts the light signal into an electric pulse for readout.

The NEAR and FAR stations on C-side were installed in 2016 [7], with all four stations operational from 2017 onward. The general locations of the AFP stations are chosen for their acceptance in fractional proton energy loss, $\xi = 1 - E_{\text{proton}}/E_{\text{beam}}$, but the precise locations are determined by constraints on free space along the beamline, away from essential beam elements and instrumentation. The total acceptance in proton fractional energy loss of AFP in 2017 data-taking was $0.02 < \xi < 0.12$. When requiring both the NEAR and FAR stations to contain a proton track (double-station reconstruction), the acceptance is reduced to $0.035 < \xi < 0.08$ in the region where station efficiencies are well understood.
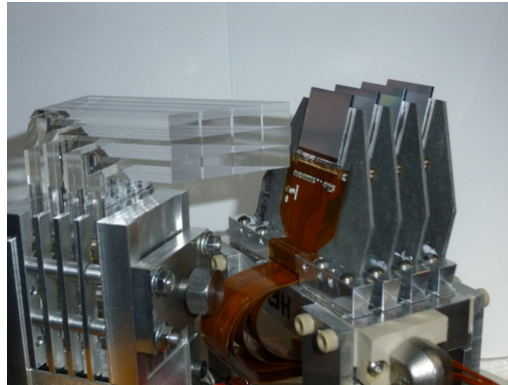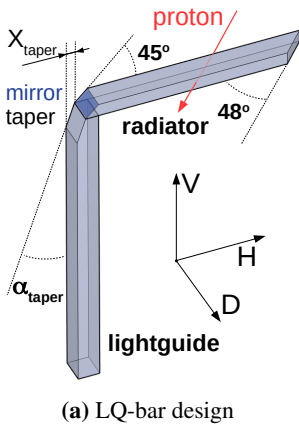

(a) LQ-bar design   **(b)** Photograph of the C-FAR SiT and ToF systems

Figure 2: (a) Design of the AFP-ToF quartz-Cherenkov LQ-bar. The L-shape with mirror tape was designed to optimise light collection whilst adhering to space constraints of the Roman Pot stations. Each arm of the bar is glued together using UV transparent glue and the end bar is attached to a micro-channel plate multi-anode photo-multiplier. (b) A photograph of the AFP SiT and ToF detectors in the C-FAR station. Both figures taken from Ref. [4].

2. Performance of the ATLAS Forward Proton detector

The performance of the AFP detector can be split into several categories, including detector alignment, LHC beam optics effects, background studies, reconstruction efficiency and resolution of SiT tracks, proton objects and time-of-flight. The components of performance with the largest impact on analysis and the areas in which current efforts are focused are discussed in the following sections.

2.1 Available data

AFP participates in both standard LHC data-taking runs with a high average number of interactions per bunch crossing, $\langle\mu\rangle$, as well as special 'low-$\langle\mu\rangle$' runs which typically have $0 < \langle\mu\rangle \leqslant 1$. The physics motivation for low-$\langle\mu\rangle$ runs is to study processes with relatively large cross-sections that require very experimentally clean environments in which to perform studies such as the study of rapidity gaps and pomeron structure in diffractive events.

The physics motivation for AFP data-taking in standard 'high-$\langle\mu\rangle$' runs is to study rarer processes with small cross-sections, in which the full available luminosity is required. Examples are photon-induced processes and central exclusive diffraction, including searches for new physics. Figure 3 shows the cumulative integrated luminosity recorded by AFP in each data-taking year, relative to that recorded by ATLAS and delivered by the LHC. In 2017 high-$\langle\mu\rangle$ runs, AFP recorded $32.0\,\text{fb}^{-1}$ of data with an average number of interactions per bunch crossing of $\langle\mu\rangle = 37.8$ [9]. After ATLAS and AFP data quality selections were applied, this dataset was reduced to $14.6\,\text{fb}^{-1}$ available for analysis. In 2022, the first year of Run 3 data-taking, AFP recorded $34.1\,\text{fb}^{-1}$ at $\langle\mu\rangle = 42.5$. After applying data-quality requirements the amount of data labelled 'good for physics analysis' ranges between 25–$30\,\text{fb}^{-1}$ depending on the central ATLAS triggers required. This increase in available data relative to 2017 highlights improved understanding of AFP operation and performance. In 2023, AFP has recorded $26.3\,\text{fb}^{-1}$ as of the end of July at $\langle\mu\rangle = 50.2$.

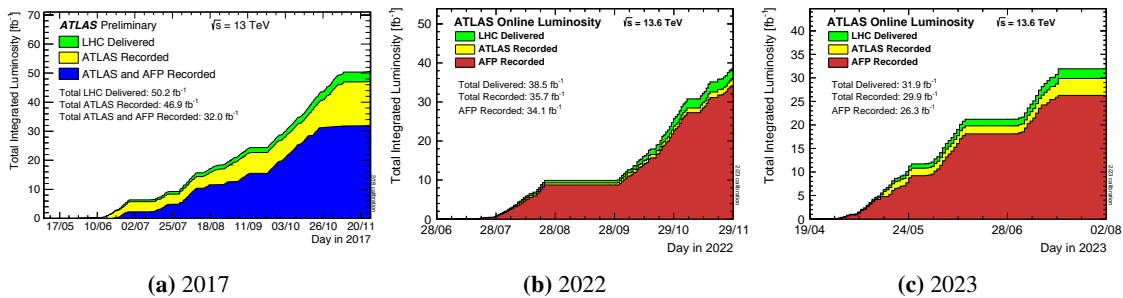**(a)** 2017   **(b)** 2022   **(c)** 2023

Figure 3: Cumulative luminosity versus time delivered to (green) and recorded by ATLAS (yellow) during stable beams for proton-proton collisions at (a) 13 TeV centre-of-mass energy in 2017 [4] and at 13.6 TeV centre-of-mass energy in (b) 2022 and (c) 2023 [8]. Also shown (blue in Run 2 and red in Run 3) is the luminosity recorded while all AFP detector stations are in physics position and AFP is being read out by the ATLAS data acquisition system.

2.2 LHC beam optics

Proton trajectories through the LHC magnetic lattice and therefore AFP acceptance and reconstructed forward proton kinematic quantities depend heavily on LHC beam optics [10]. Proton transport between IP1 and AFP is simulated in the MAD-X program [11, 12] to relate proton position in AFP to proton energy loss and determine a parameterisation $x(\xi)$. For example, the parameterisation used in Ref. [13] was $x(\xi) = -119\xi - 164\xi^2$. Systematic uncertainties on the proton position measured in AFP were determined by varying the beam crossing angle in MAD-X by $\pm 50\,\mu$rad. This approach led to a large systematic uncertainty in many Run 2 analyses. In Run 3, ongoing studies aim to determine if a better optics solution than the default LHC design values used in MAD-X can be found from a combination of database information on mechanical shifts of magnets between the ATLAS IP and AFP, tuning magnet strengths in simulation to fit trajectories to information on beam position and comparing to AFP data while accounting for known shifts in sensor position and alignment. Results of these studies will likely be used to determine the systematic uncertainty on the nominal proton transport determined by MAD-X.

2.3 Alignment

There are two components to AFP detector alignment: local 'inter-plane' alignment and global alignment of individual AFP stations. Inter-plane alignment refers to small offsets and rotations of individual SiT planes within each station. This is corrected using iterative methods based on track reconstruction in beam data and has a much smaller impact on overall proton reconstruction than global alignment, which shall be discussed here.

The accuracy of the reconstructed proton kinematics depends largely on the relative beam–detector distance of the AFP stations, which must be monitored over time due to the movement of the AFP RPs and the varying beam dynamics. The offset of the beam centre relative to the beam axis is measured using beam-based alignment (BBA) procedures [14] and cross-checked on a run-by-run basis using beam position monitor (BPM) measurements [15]. Any remaining misalignment is calculated in situ by selecting for the $\gamma\gamma \rightarrow \mu^+\mu^-$ process in data and comparing the kinematics of the central dimuon system to the kinematics of forward protons measured in AFP. In 2017, the corrections obtained are roughly $-0.4 < \delta x_{\mathrm{corr}}(s) < -0.2$ mm for all stations. A conservative uncertainty on the global alignment from these corrections was estimated to be $\pm 300\,\mu$m which partly covers neglected time dependence [13]. In Run 3, it is hoped that this uncertainty can be reduced to the order of $100\,\mu$m.

2.4 Time-of-flight performance

The ToF detector efficiencies in 2017 data-taking were measured in an AFP calibration run with $\langle\mu\rangle \sim 1$. The timing resolution was measured to be excellent at $\sigma^{\mathrm{ToF}}_{\mathrm{A\text{-}FAR}} = 20.2 \pm 4.0$ ps and $\sigma^{\mathrm{ToF}}_{\mathrm{C\text{-}FAR}} = 25.7 \pm 4.7$ ps, corresponding to an expected forward proton vertex resolution in z of $\sigma^{\mathrm{ToF}}_{\mathrm{exp.}}(\Delta z) = 5.5 \pm 2.7$ mm. However, the train efficiency was $< 7\,\%$ in both FAR stations for the majority of data-taking due to fast degradation of the PMTs in harsh operating conditions [16], rendering ToF information unusable in Run 2 physics analyses. New PMTs were installed and an out-of-vacuum solution was developed in an attempt to address ToF inefficiencies [17]. Performance

studies from early Run 3 data with $\langle\mu\rangle = 0.05$ show high single-channel efficiencies $> 85\,\%$ for all channels of both the A-FAR and C-FAR stations. Preliminary estimates of the interaction vertex spatial resolution are 8–9 mm. Example plots showing single channel efficiencies when a single SiT track is pointing to train-0 of the A-FAR station and the reconstructed interaction vertex spatial resolution when train-0 of both A-FAR and C-FAR fire are shown in Figure 4. The performance of the time-of-flight system in denser pileup environments and over time is under study.
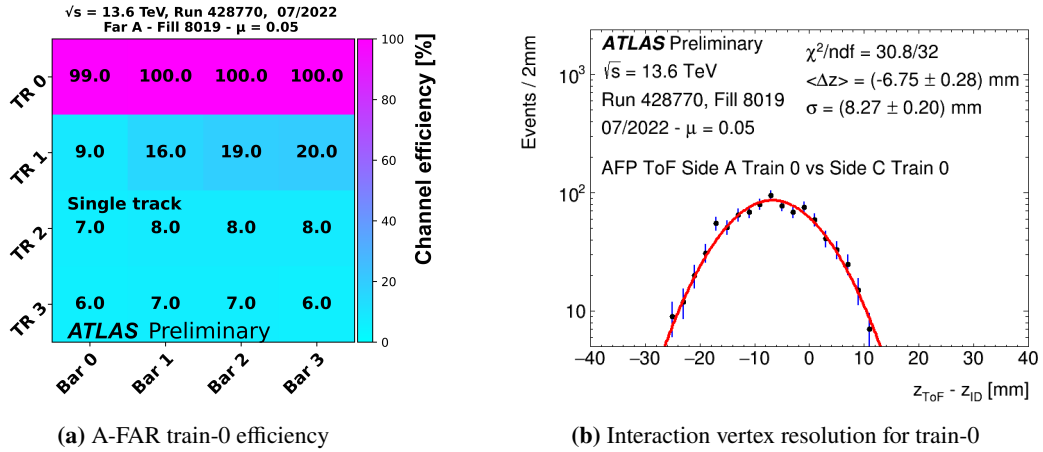

(a) A-FAR train-0 efficiency

(b) Interaction vertex resolution for train-0

Figure 4: (a) AFP-ToF channel efficiency in the A-FAR station during a single run in 2022 with $\langle\mu\rangle = 0.05$ when a single track was observed in the AFP-SiT pointing towards train-0 (TR 0). High efficiency $> 99\,\%$ is seen in the channels that the proton is expected to traverse, with some cross-talk between adjacent channels. (b) The resolution on the reconstructed proton-proton vertex position when a proton is measured in train-0 of both A-FAR and C-FAR. Both figures taken from Ref. [4].

3. Latest physics results

Some extensions to the Standard Model predict the possibility of heavy axion-like particles (ALPs), so-called in that they are pseudo-scalars that couple to two photons. A narrow resonance search in the diphoton mass spectrum in conjunction with a single or double proton tag measured in AFP was recently performed in the 2017 high-pileup proton-proton dataset at centre-of-mass energy of 13 TeV [18]. The available luminosity was $14.6\,\text{fb}^{-1}$ after ATLAS and AFP quality requirements were applied. The target ALP mass range was 150–1600 GeV, constrained by AFP acceptance. A total of 441 events passed the signal selections which is consistent with the background-only hypothesis. 95 % confidence level limits were set on the $\gamma\gamma \to a \to \gamma\gamma$ cross-section and the $a\gamma\gamma$ coupling constant, shown in Figure 5. Limits are competitive with a recent CMS-TOTEM search [19] and constrain lower in ALP mass despite a 7× smaller dataset, thanks to a novel data-driven background estimation and the inclusion of events with a single forward proton tag.

(a) Cross-section
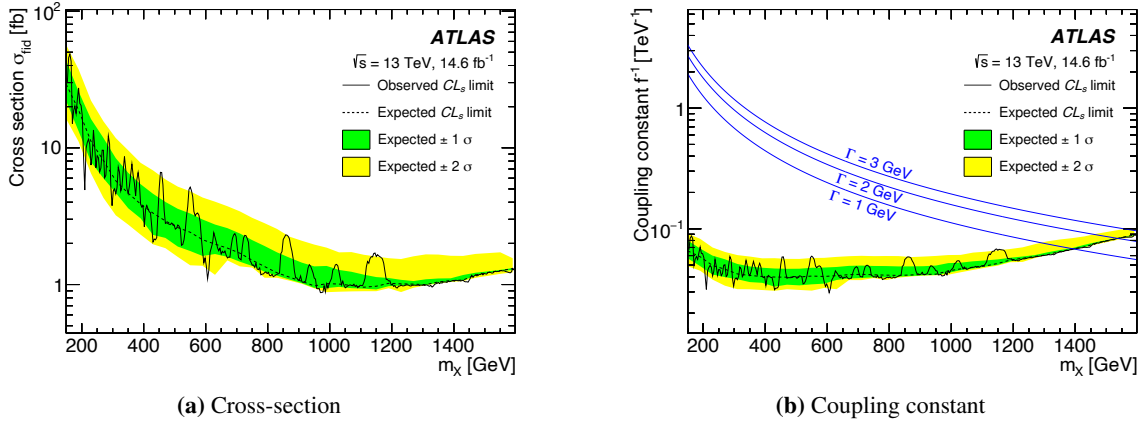

(b) Coupling constant

Figure 5: Expected and observed 95 % confidence level upper limits on (a) the signal fiducial cross section and (b) the ALP coupling constant, assuming 100 % branching ratio for ALP decay into two photons, as functions of the hypothetical ALP mass m_X. The 1σ and 2σ confidence intervals are shown by the coloured bands. Contours of the ALP natural width Γ are illustrated by the smooth blue solid lines. Figures taken from Ref. [18].

4. Conclusion

Improved understanding of AFP operation and performance in Run 3 has resulted in an unprecedented amount of data available to ATLAS physics analyses wishing to use forward protons. The dataset labelled 'good for physics' from 2022 alone more than doubles the existing 2017 dataset. Dominant systematic uncertainties relating to AFP detector performance in Run 2 arose from LHC beam optics effects and uncertainties on the global alignment of AFP stations with respect to the LHC beam. Significant work is going into understanding and reducing these uncertainties in Run 3. One of the main aims in Run 3 was improved operation of the time-of-flight system and early Run 3 data with $\langle\mu\rangle = 0.05$ show single channel efficiencies > 85 % for all channels in both the A-FAR and C-FAR stations. ToF performance in high-$\langle\mu\rangle$ runs and over time is under study. A recent search for axion-like particles was performed in the diphoton mass spectrum in conjunction with a forward proton tag in AFP [18]. Results were consistent with the background-only hypothesis and used to set 95 % confidence level limits on the ALP to diphoton cross-section and coupling constant.

References

[1] ATLAS Collaboration, *ATLAS Forward Proton Phase-I Upgrade: Technical Design Report*, *ATLAS-TDR-024; CERN-LHCC-2015-009* .

[2] ATLAS Collaboration, *The ATLAS Experiment at the CERN Large Hadron Collider*, *JINST* **3** (2008) S08003.

[3] L. Evans and P. Bryant, *LHC Machine*, *JINST* **3** (2008) S08001.

[4] ATLAS Collaboration, *AFP Figures*,
    https://twiki.cern.ch/twiki/bin/viewauth/Atlas/AFP_Figures .

[5] J. Lange, L. Adamczyk, G. Avoni, E. Banas, A. Brandt, M. Bruschi et al., *Beam tests of an
    integrated prototype of the ATLAS Forward Proton detector*, *Journal of Instrumentation* **11**
    (2016) P09005.

[6] L. Nozka, A. Brandt, M. Rijssenbeek, T. Sykora, T. Hoffman, J. Griffiths et al., *Design of
    Cherenkov bars for the optical part of the time-of-flight detector in Geant4*, *Opt. Express* **22**
    (2014) 28984.

[7] ATLAS Collaboration, *Proton tagging with the one arm AFP detector*,
    ATL-PHYS-PUB-2017-012 .

[8] ATLAS Collaboration, *Public ATLAS Luminosity Results for Run 3 of the LHC*,
    https://twiki.cern.ch/twiki/bin/view/AtlasPublic/LuminosityPublicResultsRun3 .

[9] ATLAS Collaboration, *Public ATLAS Luminosity Results for Run 2 of the LHC*,
    https://twiki.cern.ch/twiki/bin/view/AtlasPublic/LuminosityPublicResultsRun2 .

[10] M. Trzebiński, *Machine optics studies for the LHC measurements*, *SPIE Proceedings* (2014) .

[11] L. Deniau, H. Grote, G. Roy and F. Schmidt, *The MAD-X Program (Methodical Accelerator
    Design): User's Reference Manual*, *http://madx.web.cern.ch/madx/* .

[12] F. Schmidt, E. Forest and E. McIntosh, *Introduction to the polymorphic tracking code: Fibre
    bundles, polymorphic taylor types and exact tracking*, *CERN-SL-2002-044-AP,
    KEK-REPORT-2002-3* .

[13] ATLAS Collaboration, *Observation and Measurement of Forward Proton Scattering in
    Association with Lepton Pairs Produced via the Photon Fusion Mechanism at ATLAS*, *Phys.
    Rev. Lett.* **125** (2020) 261801 [2009.14537].

[14] G. Valentino, R. Aßmann, R. Bruce, S. Redaelli, A. Rossi, N. Sammut et al., *Semiautomatic
    beam-based LHC collimator alignment*, *Phys. Rev. ST Accel. Beams* **15** (2012) 051002.

[15] G. Valentino, G. Baud, R. Bruce, M. Gasior, A. Mereghetti, D. Mirarchi et al., *Final
    implementation, commissioning, and performance of embedded collimator beam position
    monitors in the Large Hadron Collider*, *Phys. Rev. Accel. Beams* **20** (2017) 081002.

[16] ATLAS Collaboration, *Performance of the ATLAS Forward Proton Time-of-Flight Detector
    in 2017*, *ATL-FWD-PUB-2021-002* .

[17] T. Sykora, *ATLAS Forward Proton Time-of-Flight Detector: LHC Run2 performance and
    experiences*, *Journal of Instrumentation* **15** (2020) C10004.

[18] ATLAS Collaboration, *Search for an axion-like particle with forward proton scattering in
    association with photon pairs at ATLAS*, *Journal of High Energy Physics* **2023** (2023)
    [2304.10953].

8

[19] CMS and TOTEM Collaborations, *Search for high-mass exclusive diphoton production with tagged protons*, *CMS-PAS-EXO-21-007, TOTEM-NOTE-2022-005* .